Bimolecular Reaction Dynamics of Thiophosgene with O(3P) Atoms

ARTICLE *in* THE JOURNAL OF PHYSICAL CHEMISTRY A · NOVEMBER 1997

Impact Factor: 2.69 · DOI: 10.1021/jp9718820

4 AUTHORS, INCLUDING:

K. Ravichandran
Bristol-Myers Squibb
2 PUBLICATIONS **7** CITATIONS
SEE PROFILE

Brad R. Weiner
University of Puerto Rico at Rio Piedras
177 PUBLICATIONS **1,492** CITATIONS
SEE PROFILE

Bimolecular Reaction Dynamics of Thiophosgene with O(^{3}P) Atoms

K. Ravichandran

Department of Chemistry, Bemidji State University, Bemidji, Minnesota 56601

Idelisa Ayala, Yasuyuki Ishikawa, and Brad R. Weiner*

Department of Chemistry, University of Puerto Rico, P.O. Box 23346, San Juan, Puerto Rico 00931

Received: June 10, 1997[⊗]

The nascent vibrational and the near-nascent rotational state distributions for the SO($X^3\Sigma^-$) product following the oxidation reaction of thiophosgene ($CSCl_2$) with O(^{3}P) have been studied by laser-induced fluorescence (LIF) spectroscopy on the ($B^3\Sigma^- - X^3\Sigma^-$) transition. O(^{3}P) atoms are produced from the 355 nm photodissociation of NO_2. The measured SO($X^3\Sigma^-$) product vibrational state distribution can be characterized as Boltzmann with a vibrational temperature $T_{vib} = 1150 \pm 55$ K corresponding to 8% of the available energy for the reaction. The statistical nature of the SO($X^3\Sigma^-$) vibrational state distribution suggests a stable intermediate for this reaction, and ab initio calculations confirm a triplet dichlorosulfine ($Cl_2CSO(^3A'')$) as a minimum on the excited triplet state potential energy surface. Statistical modeling of the observed SO($X^3\Sigma^-$) vibrational state distribution results in an available energy $E = 18$ kcal/mol, which is 1.6 kcal/mol more than the exoergicity of this reaction. On the basis of ab initio calculations in conjunction with the analysis of the experimental data in light of the statistical model, we propose little or no barrier in excess of the endothermicity for the fragmentation of the $Cl_2CSO(^3A'')$ intermediate at the exit channel. The near-nascent rotational state distribution of SO($X^3\Sigma^-$, $v'' = 0$) can be characterized by a rotational temperature $T_R = 537 \pm 35$ K corresponding to 6.7% of the available energy for the reaction. This small fraction of energy partitioned into SO($X^3\Sigma^-$) rotations may arise from a correlation between the SO rotations and the CSO bend in the $Cl_2CSO(^3A'')$ complex at the exit channel.

1. Introduction

Oxygen atoms play a central role in critical chemical environments such as combustion and atmospheric reactions.[1−3] The reactions of oxygen atoms, both in the ground state, O(^{3}P), and in the lowest electronically excited state, O(^{1}D), with hydrocarbons and hydrogen-containing molecules are known to be important in initiating stratospheric chemistry and controlling, in part, the ozone concentration.[4] Interest in the oxidation reactions of reduced sulfur species, such as OCS, CS_2, and H_2S by oxygen atoms, is due to their occurrence in the atmospheric sulfur cycle. These reactions, once initiated by an O atom, can lead to SO_2 production and ultimately yield H_2SO_4 precipitation in the atmosphere.[5] Oxidation of sulfur compounds is also critical in the combustion chemistry of sulfur-containing fuels.[6] Both kinetics and, to a lesser extent, dynamics studies have been reported for these oxidation reactions. Although the kinetics results of these reactions show good agreement across various experimental measurements, considerable uncertainty still exists about the dynamics and mechanisms of these reactions.[7] Therefore, understanding the intimate details of the oxidation reactions of sulfur compounds by O atoms is important from the atmospheric and industrial points of view.

Singleton and Cvetanović have compiled an extensive kinetic database for the reactions of sulfur compounds with O(^{3}P) atoms.[8] Based solely on the kinetic data, the reactions of O(^{3}P) with sulfur compounds are of particular dynamics interest and have been categorized into two types of mechanisms: (1) *abstraction* of sulfur or another atom from the compound by the oxygen atom; (2) *addition* of the O(^{3}P) atom to the sulfur compound. Addition can be further categorized into two subgroups: (a) *insertion* into a chemical bond, observed mostly in O(^{1}D) reactions, is spin forbidden in most O(^{3}P) reactions; (b) *displacement* of an atom or a group from the sulfur compound by the O(^{3}P) atom. Displacement usually involves initial addition of O(^{3}P) to the sulfur compound to produce an energy-rich adduct, followed by fragmentation. Since the initially formed adduct can fragment rapidly, it can be difficult to experimentally differentiate a primary abstraction and a primary addition in some of these displacement reactions. An example of such mechanistic ambiguity is the reaction of O(^{3}P) with H_2S to produce HSO and H, which could occur via a direct mechanism or by an addition−fragmentation process.[9] Recent dynamics studies in a crossed molecular beam by Casavecchia and co-workers indicate a direct mechanism for the HSO production without an H_2SO intermediate complex formation for this reaction.[10] Therefore, detailed dynamics studies will help to solve the ambiguities that remain in these reaction mechanisms.

We report here our detailed dynamics studies on the oxidation reaction of thiophosgene (Cl_2CS) with O(^{3}P) atoms by measuring the nascent SO($X^3\Sigma^-$) product rovibrational state distributions:

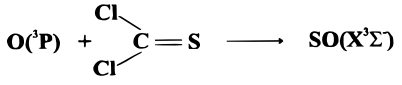

(1)

The only literature report on reaction 1 is a kinetic study by Slagle et al.,[11] where O(^{3}P) atoms were produced by microwave discharge of an O_2/He mixture and reacted with Cl_2CS in a crossed molecular jet reactor, and the primary reaction products were identified by using photoionization mass spectrometry. Kinetics measurements were carried out between 250 and 500 K in a conventional fast-flow reactor, and the O(^{3}P) atom decay

* To whom correspondence should be addressed.

[⊗] Abstract published in *Advance ACS Abstracts,* October 15, 1997.

S1089-5639(97)01882-3 CCC: $14.00

was monitored by titration with NO_2. The measured rate constants at different temperatures were fit to the Arrhenius expression $k = (3.09 \pm 0.54) \times 10^{-11} \exp(0.115 \pm 0.106 \text{ kcal mol}^{-1}/(RT))$ cm^3 molecule^{-1} s^{-1}. The strongly polarized carbon−sulfur bond in Cl_2CS and the electron-deficient character of the O(^{3}P) atom[12] led Slagle et al. to propose an electrophilic addition mechanism to produce an energy-rich triplet dichlorosulfine (Cl_2CSO) adduct as the primary step in this reaction followed by C−S bond cleavage to give SO and CCl_2 products. The above mechanism is based purely on the kinetic data. On the other hand, the SO and CCl_2 products could have resulted from a direct abstraction of S from $CSCl_2$ by the O(^{3}P) atom. Our SO($X^3\Sigma^-$) product energy disposal studies for reaction 1 described in this paper shed more light onto the proposed electrophilic addition−fragmentation mechanism.

Product energy disposal studies, especially into the vibrational degrees of freedom both in unimolecular and bimolecular cases, provide detailed information on reaction mechanisms. Recent SO($X^3\Sigma^-$) product energy disposal studies carried out in our laboratory on the reactions of carbonyl sulfide (OCS) and thiirane (C_2H_4S) with O(^{3}P) atoms provided dynamical information, such as the nature of the energy flow induced by atomic rearrangements in these reactions.[13,14] The SO($X^3\Sigma^-$) vibrational state distribution was found to be inverted with a maximum population in $v'' = 5$ and $v'' = 1$ for OCS and C_2H_4S reactions, respectively. Non-Boltzmann vibrational state distributions for the nascent SO($X^3\Sigma^-$) product suggest a direct abstraction mechanism for both reactions. The abstraction mechanisms for both reactions are further supported by crossed beam scattering studies.[15] In favorable cases, these energy disposal studies can provide structure elucidation of intermediates as well as mechanistic information for these reactions. In the current SO($X^3\Sigma^-$) energy disposal study on reaction 1, we are able to evaluate the previous conclusions about the reaction mechanism that resulted from the kinetic measurements by Slagle et al.[11] We report the nascent rovibrational state distributions of the SO($X^3\Sigma^-$) product and propose a mechanism for reaction 1 consistent with all existing data. To substantiate our experimental results, ab initio calculations to determine the possible structure(s) of the reaction intermediate(s) are reported.

2. Experimental Section

The experimental apparatus and procedure for the SO($X^3\Sigma^-$) rovibrational state distribution measurements have been described elsewhere.[16−18] The only difference in the current study is that a 355 nm laser source was used for the photolysis of NO_2 instead of 351 nm. Briefly, ground-state O(^{3}P) atoms were generated by photolysis of NO_2 using the 355 nm output of a frequency-tripled Nd:YAG laser (Continuum, Model PL7000) with typical laser fluences of 30−70 mJ/cm^2. The SO($X^3\Sigma^-$) product from reaction 1 is monitored by measuring the laser-induced fluorescence (LIF) signal of the $B^3\Sigma^- - X^3\Sigma^-$ transition in the 237−270 nm region of the spectrum. The probe dye laser (Lambda Physik FL3002; 0.25 cm^{-1} resolution) is pumped by a XeCl excimer laser (Lambda Physik, Model LPX205i) operating at 308 nm. The SO($X^3\Sigma^-$) excitation wavelength (237−270 nm) is generated by frequency doubling (β-BaB_2O_4 crystal) the dye laser fundamental output from coumarin 480 and 503 laser dyes. Both the photolysis and the probe lasers are collinearly counterpropagated along the extension arm axis of the reaction cell with a time delay of 2−5 μs between laser pulses using a pulse delay generator. LIF signals were collected at 90° relative to the laser beam axis by a high-gain photomultiplier tube (PMT) through several long-pass filters to minimize the scattered light from the photolysis and probe lasers. The output of the PMT is processed and averaged by a gated integrator, digitized, and stored in a computer for further analysis. For a fixed time delay between the photolysis and the probe lasers, the dye laser was scanned while the total fluorescence was collected to obtain the nascent LIF spectrum.

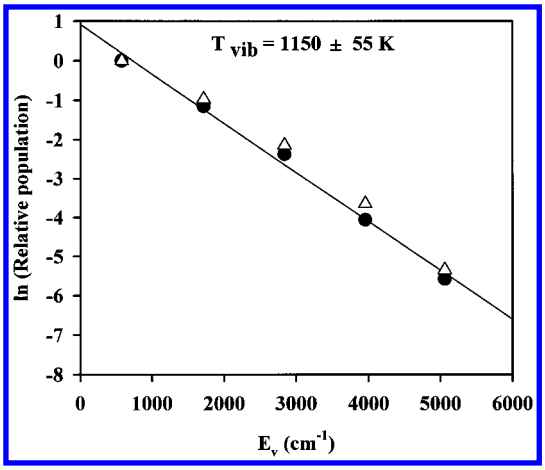

Figure 1. Semilog plots of relative nascent SO($X^3\Sigma^-$, $v'' = 0$) vibrational population versus vibrational energy E_{vib}. The symbols ● and △ represent the experimental and calculated populations, respectively. Equation 6 is used to determine the calculated population.

Cl_2CS (97%, Aldrich) was subjected to several freeze−pump−thaw cycles prior to use, and the NO_2 (98%, Matheson) precursor was used without further purification. The ratio of NO_2/Cl_2CS was typically 0.25−0.3 at a total pressure of 100−125 mTorr. The reaction cell was evacuated to 10^{-6} Torr prior to the experiments by a turbomolecular pump, but the gases were flowed by a mechanical pump during the experiments and the pressures were monitored at the exit by a capacitance manometer.

3. Results

3.1. SO($X^3\Sigma^-$) Vibrational State Distribution. The SO($X^3\Sigma^-$) product vibrational distribution from reaction 1 under two-collision conditions, i.e., 100 mTorr total reactant pressure and 2 μs delay between the photolysis excimer and probe dye lasers, was obtained by integrating the area of the LIF spectra for the vibronic transitions terminating on the $v' = 1$ level of the B state (1, $v'' = 0-4$) and normalizing for their respective Franck−Condon (FC) factors.[19] The vibronic bands were assigned using the spectroscopic constants reported by Colin.[20,21] The experimentally determined SO($X^3\Sigma^-$) product vibrational state distribution under two-collision conditions is shown in Figure 1. Since vibrational relaxation occurs with more collisions (typically once every 100−1000 collisions) for SO($X^3\Sigma^-$, $v'' = 2$) with several different polyatomic collisional partners,[22] the measured vibrational state distribution for SO($X^3\Sigma^-$) for reaction 1 can be considered as nascent. Figure 1 demonstrates that the nascent SO($X^3\Sigma^-$) vibrational state distribution from reaction 1 can be characterized as Boltzmann with a vibrational temperature, T_{vib}, of 1150 ± 55 K. T_{vib} was obtained from the slope of the ln(N_v) vs SO vibrational energy (E_{vib}) plot as shown in Figure 1.

3.2. SO($X^3\Sigma^-$) Rotational State Distribution. The SO($B^3\Sigma^- - X^3\Sigma^-$) LIF spectra have been used for the measurement of rotational state distributions for the SO product following the reaction of O(^{3}P) with Cl_2CS. The rotational levels of each of the $^3\Sigma^-$ electronic states are split into three spin components by spin−orbit interactions, namely, F_1 for $J = N + 1$, F_2 for $J = N$, and F_3 for $J = N - 1$. Since SO($X^3\Sigma^-$) belongs to the Hund's case b, only six branches, namely, P_{11}, P_{22}, P_{33}, R_{11},

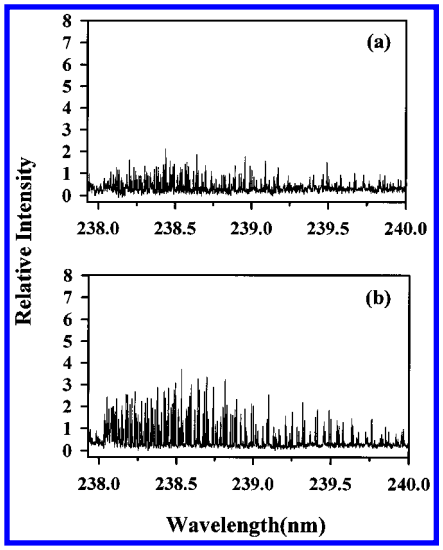

Figure 2. Rotationally resolved LIF spectrum of the SO($B^3\Sigma^-$, $-v' = 1 - X^3\Sigma^-$, $v'' = 0$) transition following the reaction of O(^{3}P) with $CSCl_2$: (a) 0.02 Torr of NO_2 and 0.08 Torr of $CSCl_2$ with 2 μs delay between photolysis and probe lasers; (b) 0.02 Torr of NO_2 and 0.08 Torr of $CSCl_2$ with 5 μs delay between photolysis and probe lasers. The two spectra correspond to about two and five gas kinetic collisions, respectively.

R_{22}, and R_{33} in SO($B^3\Sigma^- - X^3\Sigma^-$) rovibronic transitions have strong intensities. The measured rotationally resolved LIF excitation spectrum of SO($B^3\Sigma^-$, $v' = 1 - X^3\Sigma^-$, $v'' = 0$) after two and five collisions from reaction 1 is shown in Figure 2. Although the overall intensity for the five-collision spectrum is greater than the two-collision one, we did not notice any significant change in the distribution of intensities, which probably suggests that the reaction is still occurring. The assignment of the spectrum is based on the calculated line positions using Colin's spectroscopic constants,[20,21] and the difference between the calculated line positions and the experimental measurements are within 0.005 nm.

The rotational state populations in a given vibrational band, $P(N'')$, are determined by normalizing the LIF signal intensity of the transition by the Hönl−London factor[23] and the rotational degeneracy. The rotational line positions of the $F_1'-F_1''$ transitions overlap with the $F_3' - F_3''$ transitions at low N and cannot always be rotationally resolved with our probe laser line widths. Therefore, the $F_2'-F_2''$ transitions are used to measure the rotational state populations.

The measured $P(N'')$ from the LIF excitation spectra can be described by the following Boltzmann expression

$$P(N'')/[2J'' + 1] = \exp[-B_v N''(N'' + 1)/(k_B T_R)] \quad (2)$$

where B_v is the rotational constant of the given vibrational state, k_B the Boltzmann constant, $2J'' + 1$ the rotational degeneracy, and T_R the rotational temperature. If a plot of $\ln[P(N'')/(2J'' + 1)]$ versus $BN''(N'' + 1)$ can be fit to a straight line, then the slope corresponds to $-1/(kT_R)$, from which T_R can be determined. Figure 3 shows a Boltzmann plot of the rotational state population of SO($X^3\Sigma^-$, $v'' = 0$) following two and five gas kinetic collisions, and the straight line corresponds to the linear least-squares best fit to the points. The rotational temperatures obtained by the above method are 535 ± 65 and 460 ± 52 K for two and five gas kinetic collisions, respectively.

4. Discussion

The reaction shown in eq 1 is exothermic ($\Delta H_{RXN} = -13$ kcal/mol). The thermochemistry and the two other possible

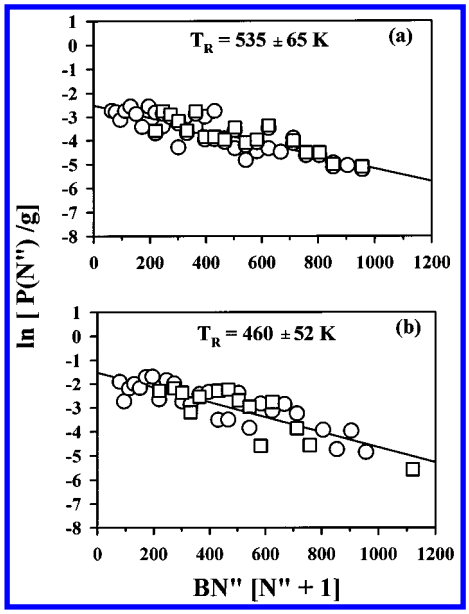

Figure 3. Semilog plots of the relative population in the rotational levels of SO($X^3\Sigma^-$, $v'' = 0$), corrected for the rotational degeneracy $g(N'') = (2N'' + 1)$, versus the rotational energy $BN''(N'' + 1)$ corresponding to the spectra shown in (a) and (b) of Figure 2. The symbols ○ and □ represent P_{22} and R_{22} rovibronic transitions, respectively. The solid lines are the linear least-squares fits to the data and correspond to Boltzmann temperatures (see eq 2) of 535 ± 65 and 460 ± 52 K, respectively.

product channels for SO production from the title reaction are

$$O(^3P) + CSCl_2 \rightarrow SO(a^1\Delta) + CCl_2(^1A_1) \qquad \Delta H_{RXN} = 5.1 \text{ kcal/mol} \quad (3)$$

$$\rightarrow SO(X^3\Sigma^-) + CCl_2(^3B_1) \qquad \Delta H_{RXN} = -1 \text{ kcal/mol} \quad (4)$$

There are some uncertainties in the ΔH_f^0 at 298 K for $CSCl_2$ and $CCl_2(^1A_1$ and $^3B_1)$. For the current study, they were obtained from the most recent literature sources.[24,25] Relative energies from the computed minimum for the reactants, intermediate, and products were also obtained by using the Gaussian-2 (G2) theoretical procedure,[26] and excellent agreement was found between the experimental and computed heat of reaction ($\Delta H_{RXN} = -12.99$ kcal/mol) for eq 1. We have included a slightly endothermic channel (reaction 3) because of the possibility of excess kinetic energy in the reactants. Reaction 4, on the other hand, can be neglected based on spin conservation rules in our studies.

Our LIF measurement of SO($X^3\Sigma^-$) under two-collision conditions (cf. Figure 2) in different vibrational levels demonstrates that reaction 1 is operative. Under these conditions, relaxation of SO($a^1\Delta$) to SO($X^3\Sigma^-$), if produced from reaction 3, is negligible owing to the slowness of the relaxation.[27] Therefore, the measured vibrational state distribution of SO($X^3\Sigma^-$) from reaction 1 under our experimental conditions is believed to be nascent. The measured rotational temperatures are 535 ± 65 and 460 ± 52 K for SO($^3\Sigma^-$, $v'' = 0$) under two and five gas-kinetic collisions, respectively. These two temperatures are not significantly different, i.e., they overlap within the experimental error limits, and it is therefore difficult to attribute the small change in the temperature to rotational relaxation within one electronic manifold. Since rotational relaxation occur with rate constants in excess of the collisional rate constant based on simple gas kinetic theory, our measured rotational temperature under the two-collision condition is only near-nascent.

To arrive at the percent energy disposed to the $SO(X^3\Sigma^-)$ product in reaction 1, it is important to know the total available energy (E_{av}) in this reaction, which includes the kinetic energy of $O(^3P)$ from the 355 nm photodissociation of NO_2. The center of mass (c.m.) kinetic energy of $O(^3P)$ atom from this photodissociation process has been well-studied in the past.[28,29] It is known that this photodissociation process results in 4.5 kcal/mol as c.m. kinetic energy for $O(^3P)$ corresponding to the formation of $NO(X^2\Pi_{1/2}, v = 0)$ and 1.7 kcal/mol corresponding to $NO(X^2\Pi_{1/2}, v = 1)$. The maximum total energy available in reaction 1 is 17.5 kcal/mol, which includes kinetic energy from $O(^3P)$ corresponding to the $NO(X^2\Pi_{1/2}, v = 0)$ channel, and an average c.m. collision energy $\langle E_{coll}\rangle$ of 3.4 kcal/mol for $O(^3P)$ is obtained for reaction 1 from the relative yields of $NO(X^2\Pi_{1/2}, v = 0)/NO(X^2\Pi_{1/2}, v = 1)$ from the 355 nm photolysis of NO_2.[30] This $\langle E_{coll}\rangle$ results in E_{av} of 16.4 kcal/mol, which can be partitioned among the $SO(X^3\Sigma^-)$ and $CCl_2(^1A_1)$ products' degrees of freedom in reaction 1.

Since energy disposed into the vibrational modes of the product and the qualitative shapes of product vibrational state distributions are known to serve as a diagnostic for reaction mechanisms, we will consider them first. The measured nascent vibrational state distribution of the $SO(X^3\Sigma^-)$ product from reaction 1 within two gas kinetic collisions (using the data shown in Figure 1) can be used to calculate the energy partitioned into the $SO(X^3\Sigma^-)$ vibrational degree of freedom from the following expression: $E_{vib} = \sum c_v(E_v - E_0)$, where E_0 is the zero-point energy, E_v is the vibrational energy for state v'', and c_v is the fractional population in each vibrational level. This average nascent vibrational energy was calculated to be 1.3 kcal/mol, which corresponds to 8% of E_{av}. As a result of a Boltzmann type vibrational distribution for the $SO(X^3\Sigma^-)$ product, one possible explanation is that the reaction proceeds via a long-lived intermediate and all modes of this intermediate participate equally in product formation.

Owing to the electrophilic nature of $O(^3P)$, the high charge density on the sulfur atom in Cl_2CS, and the spin conservation for the reaction, we propose the formation of the same triplet dichlorosulfine (Cl_2CSO) intermediate as that of Slagle et al.[11] to be the primary process. The primary step is the attack of $O(^3P)$ on the sulfur end of Cl_2CS to produce an energy-rich, triplet dichlorosulfine (Cl_2CSO) intermediate. The Cl_2CSO intermediate must involve at least one of the lone pairs of electrons from the sulfur atom transferring to the $O(^3P)$ atom, thereby resulting in the two resonating structures, as shown in reaction 5:

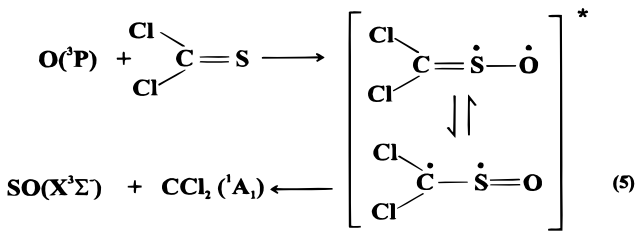

(5)

This triplet Cl_2CSO intermediate then undergoes a C−S bond cleavage to give $SO(X^3\Sigma^-)$ and $CCl_2(^1A_1)$ products. The overall reaction mechanism is given in eq 5.

Since the kinetics experiments by Slagle et al.[11] were carried out at high pressures, it seems likely that the rate-determining step must be the one that involves overcoming the barrier in the entrance channel of this reaction to produce the triplet Cl_2CSO intermediate. A near-zero activation energy (-0.115 ± 0.106 kcal/mol) was reported for this reaction in their work. In our experiments the reaction overcomes this small barrier, if any, by the c.m. kinetic energy imparted to the $O(^3P)$ atom from the 355 nm photodissociation of NO_2.

TABLE 1: Calculated ab Initio (MP2/6-311G* Level) Geometric Parameters for Cl_2CSO (Excited $^3A''$ State and Ground $^1A'$ State) along with Electron Diffraction Data[c]

	this work		expt[a]
	$Cl_2CSO(^3A'')$	$Cl_2CSO(^1A')$	$Cl_2CSO(^1A')$
S═O	1.474	1.484	1.453
S═C	1.785	1.667	1.618
C−Cl	1.705	1.702 (cis)	1.718 (cis)
	1.705	1.720 (trans)	1.718 (trans)
∠CSO	109.4	113.4	113.8
∠ClCSO (dihedral)	118.7[b]		
$\angle SCCl_{cis}$		122.2	126.2
$\angle SCCl_{trans}$		118.5	118.8

[a] Reference 33. [b] See Figure 4. [c] Bond lengths are given in angstroms and bond angles in degrees.

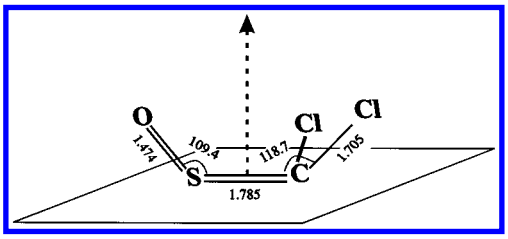

Figure 4. Calculated ab initio (MP2/6-311G* level) geometry for $Cl_2CSO(^3A'')$ intermediate. Bond lengths and bond angles for the intermediate are given in Table 1.

To understand the intimate details of the proposed mechanism, we need to get a better grasp of the structure of the triplet Cl_2CSO intermediate. Ground-state sulfines are known to be relatively stable in the gas phase, even though the simplest moiety, H_2CSO, is quite unstable.[31,32] Several substituted sulfines, including the ground state of Cl_2CSO, have been studied recently in the gas phase by electron diffraction and were found to be planar with a C_s symmetry.[33] Ab initio calculations of ground-state H_2CSO have revealed the planar structure for this molecule.[34] To the best of our knowledge, the structure of the excited triplet Cl_2CSO has not been reported. Our ab initio computational efforts employing the Gaussian 94 suite of programs[35] find the minimum energy geometries for both ground and excited triplet states of Cl_2CSO at the MP2/6-311G* level of theory. The calculated triplet excited-state geometry for the Cl_2CSO intermediate provides a qualitative picture into the dynamics and mechanism for the title reaction.

The results of our calculations for the planar ($^1A'$) ground-state Cl_2CSO along with the gas-phase geometric parameters derived by Liedle et al. using electron diffraction[33] are given in Table 1. Our calculated geometry for ground-state Cl_2CSO is in excellent agreement (within ±3%) with that of the electron diffraction experiments, and this gives a measure of confidence in our excited-state structure. Our ab initio calculations on the triplet excited ($^3A''$) state of Cl_2CSO reveal that the molecule is nonplanar (puckered structure) compared to the planar ground-state geometry. This is not surprising, since the structure of ground-state thiophosgene (Cl_2CS) is planar with a C_{2v} symmetry and the first excited triplet state ($^3A_2$) is nonplanar with a 32° out-of-plane bending angle.[36] In the case of Cl_2CSO, the planarity of the excited triplet state is lost by virtue of the two Cl atoms and the O atom pointing outward in the same direction from the C−S bond axis of the molecule. The calculated optimized geometry (C_s symmetry) for the triplet excited state of Cl_2CSO, given in Figure 4, demonstrates the nonplanarity of this molecule. Note that this energy minimum corresponds to the cis form of this molecule, and attempts made to find the

energy minimum for the trans, with the two Cl and O atoms pointing in opposite direction from the C−S bond axis, only reverted back to the cis conformation. Our calculations for the ground state and excited triplet Cl_2CSO intermediate, without any restrictions imposed on the structure and symmetry, resulted in $^1A'$ and $^3A''$ designations for these states, respectively. The G-2 calculated energy difference between $^1A'$ and $^3A''$ states for Cl_2CSO is 36 kcal/mol. This large energy difference suggests that reaction 1 proceeds exclusively via the $^3A''$ surface of Cl_2CSO with little or no participation from the $^1A'$ surface.

Since reaction 1 resulted in a Boltzmann-like $SO(X^3\Sigma^-)$ product vibrational distribution, a statistical energy disposal model developed by Bogan et al.[37] and Rosenfeld and co-workers[38] was employed for comparison. In this model, the probability $f(\epsilon, E)$ of producing the $SO(X^3\Sigma^-)$ with vibrational energy ϵ for a given available energy E is given by the equation

$$f(\epsilon, E) = \frac{N_{SO}(\epsilon)\int_{E_t}^{E-\epsilon} P_r(E-\epsilon-E_t)\sqrt{E_t}\,dE_t}{\sum_{\epsilon=0}^{E} N_{SO}(\epsilon)\int_{E_t}^{E-\epsilon} P_r(E-\epsilon-E_t)\sqrt{E_t}\,dE_t} \quad (6)$$

where $N_{SO}(\epsilon)$ is the vibrational density of states of $SO(X^3\Sigma^-)$ at vibrational energy ϵ, which can be calculated from the harmonic oscillator approximation. $P_r(E-\epsilon-E_t)$ is the total number of states corresponding to the vibrational and all active rotational degrees of freedom of the other product, namely, CCl_2-($^1A_1$) at energy $(E-\epsilon-E_t)$ where E_t is the translational energy. $P_r(E)$ is calculated by using the Whitten−Rabinovitch semiclassical algorithm.[39] It should be noted that this statistical model allows us to compare our experimental results to what would be expected in the limit of statistical energy partitioning to the $SO(X^3\Sigma^-)$ product and cannot function as a unique model for the dynamics of reaction 1. This model requires the $SO(X^3\Sigma^-)$ and $CCl_2(^1A_1)$ products' vibrational frequencies and an available energy E, which is a fitting parameter. This energy can be either the total exoergicity of the reaction, i.e., 16.4 kcal/mol, if the reaction is only controlled by the small entrance channel barrier or anything different than this if the Cl_2CSO intermediate has an exit channel barrier. Since the global potential energy surface and the transition state structures for $Cl_2CSO(^3A'')$ were not calculated, it is rather difficult to estimate the barrier, if any, for this intermediate. An approximate potential energy profile for reaction 5, including the possibility of any exit channel barrier, was deduced from the calculated $SO(X^3\Sigma^-)$ vibrational state distributions based on the statistical model and from the relative energies obtained from the computed minimum for the reactants, intermediate, and products by the G-2 theoretical procedure.[26] Our G-2 calculations resulted in a 46 kcal/mol energy separation between the reactants and $Cl_2CSO(^3A'')$ intermediate. This result strongly favors a bound state for this species.

The calculated $SO(X^3\Sigma^-)$ product vibrational state distribution using the statistical model is shown in Figure 1. The vibrational frequencies for the $CCl_2(^1A_1)$ product are obtained from the recent rotationally resolved spectral studies for this molecule by Clouthier and co-workers.[40] Our experimental data fit well to the calculated distributions only when the available energy E in eq 6 is 18 kcal/mol, in good agreement with the 16.4 kcal/mol exoergicity of reaction 1. This results in a transition state for the $Cl_2CSO(^3A'')$ intermediate to be roughly equal to the energy of the products (shown in dotted lines in Figure 5) in the exit channel. Thus, the reaction has little or no barrier associated with the exit channel for the $Cl_2CSO(^3A'')$ intermediate to the extent that this model is an accurate representation.

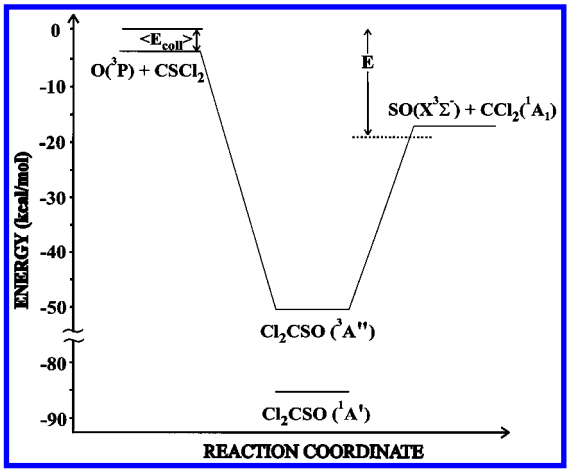

Figure 5. Calculated energy level diagram for $O(^3P) + CSCl_2$ reaction based on the ab initio calculations and statistical model. Refer to text for details.

The entire potential energy profile based on the above results for reaction 5 is given in Figure 5.

The average near-nascent rotational energy E_{rot} disposed to the $SO(X^3\Sigma^-)$ product in reaction 1 is estimated from $k_B T_{rot}$, where T_{rot} is the average of the rotational temperatures of $SO(X^3\Sigma^-, v'' = 0-4)$ under two gas kinetic collisions. The calculated T_{rot} is 537 ± 65 K, which results in E_{rot} of 1.07 kcal, corresponding to 6.7% of E_{av}. This small percentage (6.7%) of available energy disposed into the rotational degree of freedom in $SO(X^3\Sigma^-)$ and with little or no barrier predicted for the $Cl_2CSO(^3A'')$ intermediate suggests that the SO rotations in the complex probably correlates with the CSO bend in the exit channel. Moreover, the center of mass in the Cl_2CSO-($^3A''$) intermediate lies more toward the carbon end of this molecule because of the heavy Cl atoms bonded to it, and therefore, the other product, namely, $CCl_2(^1A_1)$, should carry most of the available energy in its internal degrees of freedom. LIF experiments are currently underway to detect the $CCl_2(^1A_1)$ product in this reaction.

5. Summary and Conclusions

We have reported our detailed experimental and theoretical studies of the dynamics of the reaction of $O(^3P)$ with $CSCl_2$. Our results and analysis are summarized as follows.

(1) Nascent vibrational and near-nascent rotational state distributions of the $SO(X^3\Sigma^-)$ product have been measured by using laser-induced fluorescence spectroscopy following the 355 nm photolysis of NO_2 in the presence of $CSCl_2$. The vibrational state distribution of the $SO(X^3\Sigma^-)$ product was found to be Boltzmann (see Figure 1) with a temperature $T_{vib} = 1150 \pm 55$ K corresponding to 8% of the available energy for this reaction. The measured Boltzmann vibrational distribution is consistent with a long-lived $Cl_2CSO(^3A'')$ intermediate, in agreement with the previous kinetics measurements made on this reaction system.[11] The SO is produced rotationally cold with a $T_{rot} = 537 \pm 65$ K (i.e., $E_{rot} = 1.07$ kcal/mol), corresponding to 6.7% of E_{av}.

(2) The Gaussian-2 theoretical procedure, based on ab initio correlated methods, has been applied to reactants, products, and intermediates in order to evaluate their relative stabilities. For the reactants and products, the calculated results are in strong agreement with previously measured experimental values. Ab initio correlated calculations have been employed to determine the structures of the $^3A''$ intermediate and the $^1A'$ ground state of Cl_2CSO.

(3) The large energy difference of 36 kcal/mol calculated between the $^3A''$ intermediate and $^1A'$ ground-state Cl_2CSO indicates that the reaction might proceed exclusively via a triplet potential energy surface in Cl_2CSO. The calculated vibrational energy distribution for the $SO(X^3\Sigma^-)$ product, based on a statistical energy-partitioning model in conjunction with the G-2 calculated single-point energies for the reactants, products, and the $Cl_2CSO(^3A'')$ intermediate, suggests that the reaction has little or no barrier in the exit channel.

(4) The detailed dynamics studies described here are best explained in terms of an addition−fragmentation mechanism similar to that proposed in previous kinetic studies of this reaction.[11]

Acknowledgment. We acknowledge the generous support of this project by the U.S. Department of Energy (Grant No. DE-FG02-94ER75764). Partial support has also been provided by NASA through Grants NCCW-0056 and NAGW-4059. All the experiments performed here were done in conjunction with the Puerto Rico Laser and Spectroscopy Facility at the University of Puerto Rico, under the auspices of the NSF-EPSCoR and NIH-RCMI programs. The calculations were carried out at the RCMI Center for Molecular Modelling and Computational Chemistry.

References and Notes

(1) Levine, J. S. *The Photochemistry of Atmospheres*; Academic Press, Inc.: New York, 1985.
(2) Wayne, R. P. *Chemistry of Atmosphere*, Oxford University Press: Oxford, 1991.
(3) Warneck, P. *Chemistry of Natural Atmosphere*; Academic Press, Inc.: New York, 1988.
(4) Force, A. P.; Wiesenfeld, J. R. *J. Phys. Chem*. **1981**, *85*, 782.
(5) Tyndall, G. S.; Ravishankara, A. R. *Int. J. Chem. Kinet*. **1991**, *23*, 483, and references therein.
(6) (a) Brown, S. D.; Ismail, K.; Thomas, K. M. *Energy Fuels* **1995**, *9*, 1104. (b) Farago, Z. *Combust. Sci. Technol*. **1991**, *79*, 73.
(7) DeMore, W. B.; Golden, D. M.; Hampson, R. F.; Howard, C. J.; Kurylo, M. J.; Molina, M. J.; Ravishankara, A. R.; Sander, S. P. *JPL Publ.* **1994**, *December 15*, 94-26 and references therein.
(8) Singleton, D.; Cvetanović, R. J. *J. Phys. Chem. Ref. Data* **1988**, *17*, 1377.
(9) (a) Singleton, D. L.; Irwin, R. S.; Nip. W. S.; Cvetanović, R. J. *J. Phys. Chem*. **1979**, *83*, 2195. (b) Singleton, D. L.; Paraskevopoulos, G.; Irwin, R. S. *J. Phys. Chem*. **1982**, *86*, 2605. (c) Slagle, I. R.; Baiocchi, F.; Gutman, D. *J. Phys. Chem*. **1978**, *82*, 1333. (d) Davidson, F. E.; Clemo, A. R.; Duncan, G. L.; Browett, R. J.; Hobson, J. H.; Grice. R. *Mol. Phys.* **1982**, *46*, 33.
(10) Alagia, M.; Balucani, N.; Casavecchia, P.; Stranges, D.; Volpi, G. G. *J. Chem. Soc., Faraday Trans*. **1995**, *91*, 575.
(11) Slagle, I. R.; Gutman, D. *Int. J. Chem. Kinet*. **1979**, *11*, 453.
(12) Cvetanović, R. J. *Can. J. Chem*. **1960**, *38*, 1678.
(13) Chen, X.; Wu, F.; Weiner, B. R. *Chem. Phys. Lett*. **1995**, *247*, 313.
(14) Ravichandran, K.; Gong, Y.; Wu, F.; Weiner, B. R. *Chem. Phys. Lett*. **1996**, *256*, 348.
(15) (a) Rochford, J. J.; Powell, L. J.; Grice, R. *J. Phys. Chem.* **1995**, *99*, 15369. (b) Gao, X.; Hall, M. P.; Smith, D. J.; Grice, R. *J. Phys. Chem.* **1997**, *101*, 187.
(16) Wang, H.; Chen, X.; Weiner, B. R. *J. Phys. Chem*. **1993**, *97*, 12260.
(17) Chen, X.; Asmar, F.; Wang, H.; Weiner, B. R. *J. Phys. Chem*. **1991**, *95*, 6415.
(18) Wang, H. Chen, X.; Weiner, B. R. *Chem. Phys. Lett*. **1993**, *216*, 537.
(19) Smith, W. H.; Liszt, H. S. *J. Quant. Spectrosc. Radiat. Transfer* **1975**, *11*, 45.
(20) Colin, R. *Can. J. Phys*. **1969**, *47*, 979.
(21) Colin, R. *J. Chem. Soc., Faraday Trans. 2* **1982**, *78*, 1139.
(22) Gu, X.; Chen, X.; Weiner, B. R. Unpublished results.
(23) Tatum, J. B. *Can. J. Phys*. **1966**, *44*, 2944.
(24) Joshi, R. M. *J. Macromol. Sci., Chem.* **1979**, *A13* (7), 1015.
(25) Sharon, G. L.; Karpas, Z.; Liebman, J. *J. Am. Chem. Soc*. **1985**, *107*, 6089.
(26) Curtiss, L. A.; Raghavachari, K.; Trucks, G. W.; Pople, J. A. *J. Chem. Phys.* **1981**, *94*, 7221.
(27) (a) Barnes, I.; Beckar, K. H.; Fink, E. H. *Chem. Phys. Lett*. **1979**, *67*, 310. (b) Kanamori, H.; Tiemann, E.; Hirota, E. *J. Chem. Phys*. **1988**, *89*, 621.
(28) Busch, G. E.; Wilson, K. R. *J. Chem. Phys*. **1972**, *56*, 3626.
(29) Hradil, V. P.; Suzuki, T.; Hewitt, S. A. *J. Chem. Phys*. **1993**, *99*, 4455.
(30) Harrison, J. A.; Yang, X.; Rösslein, M.; Felder, P.; Huber. J. R. *J. Phys. Chem*. **1994**, *98*, 12260.
(31) Powers, D. E.; Arrington, C. A.; Harris, W. C.; Block, E.; Kalasinsky, V. F. *J. Phys. Chem.* **1979**, *83*, 1890.
(32) Block, E.; Penn, R. E.; Olsen, R. J.; Shervin, P. F. *J. Am. Chem. Soc*. **1976**, *98*, 1264.
(33) Liedle, S.; Oberhammer, H.; Fritz, H.; Sundermeyer, W. *J. Mol. Struct.* **1990**, *216*, 171.
(34) Ruttink, P. J. A.; Burgers, P. C.; Francis, J. T.; Terlouw, J. K. *J. Phys. Chem*. **1996**, *100*, 9694.
(35) Frisch, M. J.; Trucks, G. W.; Schlegel, H. B.; Gill, P. M. W.; Johnson, B. G.; Robb, M. A.; Cheeseman, J. R.; Keith, T. A.; Petersson, G. A.; Montgomery, J. A.; Raghavachari, K.; Al-Laham, M. A.; Zakrzewski, V. G.; Ortiz, J. V.; Foresman, J. B.; Cioslowski, J.; Stefanov, B. B.; Nanayakkara, A.; Challacombe, M.; Peng, C. Y.; Ayala, P. Y.; Chen, W.; Wong, M. W.; Andres, J. L.; Replogle, E. S.; Gomperts, R.; Martin, R. L.; Fox, D. J.; Binkley, J. S.; Defrees, D. J.; Baker, J.; Stewart, J. P.; Head-Gordon, M.; Gonzalez, C.; Pople, J. A. *Gaussian 94*, Revision A.1; Gaussian, Inc.: Pittsburgh, 1995.
(36) Clouthier, D. J.; Moule, D. C. *J. Mol. Spectrosc*. **1981**, *87*, 471.
(37) Bogan, D. J.; Setser, D. W. *J. Chem. Phys.* **1976**, *64*, 586.
(38) Rosenfeld, R. N.; Weiner, B. R. *J. Am. Chem. Soc.* **1983**, *105*, 3485.
(39) Whitten, G. Z.; Rabinovitch, B. S. *J. Chem. Phys*. **1964**, *41*, 1883.
(40) Clouthier, D. J.; Karolczak, J. *J. Chem. Phys*. **1991**, *94*, 1.